Chemical Geology 266 (2009) 306–319

Contents lists available at ScienceDirect

Chemical Geology

journal homepage: www.elsevier.com/locate/chemgeo

Fluid source-based modeling of melt initiation within the subduction zone mantle wedge: Implications for geochemical trends in arc lavas

Laura Baker Hebert *[,1], Paul Asimow, Paula Antoshechkina

California Institute of Technology; Pasadena, CA 91125, United States

ARTICLE INFO

Article history:
Received 30 August 2008
Received in revised form 15 April 2009
Accepted 15 June 2009

Editor: D.B. Dingwell

Keywords:
Costa Rica
Izu–Bonin
Subduction
Volcanic front
Cross-arc trends
GyPSM-S

ABSTRACT

The GyPSM-S (*G*eodynamic and *P*etrological *Sy*nthesis *M*odel for *S*ubduction) scheme couples a petrological model with a 2-D thermal and variable viscosity flow model to describe and compare fundamental processes occurring within the subduction mantle wedge, including the development of a low-viscosity channel (LVC) (Hebert et al., 2009, *Earth and Planetary Science Letters*, v. 278, p. 243–256). Here we supplement the basic coupled model result with more sophisticated treatments of trace element partitioning in the fluid phase and melt transport regimes. We investigate the influences of slab fluid source lithology and fluid transport mechanisms on melt geochemistry, the implications of mantle source depletion related to fluid fluxing, and potential melt migration processes. This study describes two model cases that can be compared to geochemical datasets for the Izu–Bonin intra-oceanic subduction system and the Central Costa Rican part of the Central American arc. We find that there is a progression of geochemical characteristics described in studies of cross-arc and along-arc lavas that can be approximated assuming (i) limited fluid–rock interaction within the mantle wedge and (ii) that melt migration preserves the spatial distinction among melts initiated in different areas of the wedge. Specifically, volcanic front lavas have significant contributions from shallower slab fluid sources, and rear-arc lavas have significant contributions from deeper slab fluid sources. Evidence for limited fluid–rock interaction could imply either a rapid fluid transport mechanism or a fluid-dominated trace element budget within the LVC. Although we do not include a back-arc in these models, interpretations of the results lead to several potential mechanisms to explain hydrous inputs to back-arc source regions.

1. Introduction

Melting within the mantle at convergent plate boundaries is an important problem that has been addressed through analyses of lavas and xenoliths collected at the surface (Plank and Langmuir, 1988), interpretations of seismic imaging results (Zhao, 2001; Hasegawa et al., 2005), numerical modeling (Gerya and Yuen, 2003; Iwamori, 2007; Hebert et al., 2009) and experimental investigations (Gaetani and Grove, 1998, 2003). Fluxing of the mantle by components derived from heterogeneous slab sources, the potential for significant crustal contamination, sources of initial and progressive mantle source depletion, and a complex pressure and temperature structure are some of the complicating factors for understanding melt initiation and chemistry within the sub-arc mantle wedge.

Major element abundances in most modern arc lavas are generally thought to be derived from partial melting of the wedge peridotite above the slab, but large-ion lithophile elements (LILE) and other incompatible elements can be traced to slab-derived influences such as sediment melting (Plank and Langmuir, 1993; Elliott et al., 1997), dehydration of the altered oceanic crust (AOC) (Ishikawa and Tera, 1999), and/or dehydration of subducting serpentinized lithosphere (Ulmer and Trommsdorf, 1995; Schmidt and Poli, 1998). In general, convergent margins involve lavas that are enriched in incompatible fluid-mobile elements (Rb, Ba, U, K, Sr, Pb) and depleted in incompatible high field strength elements (HFSE) (Nb, Zr, Ta) and heavy rare-earth elements (HREE) (Arculus, 1994; Hawkesworth et al., 1997; Stern et al., 2006; others), suggesting a significant connection between fluids, mantle source bulk composition, and melt production. However, straightforward interpretation of the geochemistry can be somewhat obscured by the complexity of slab sources and the potential for multi-stage melting (leading to progressive depletion) events.

The depth interval and the magnitude of fluid release from the subducting plate are a function of parameters such as slab age and convergence velocity (Peacock, 1990; Iwamori, 1998; Hebert et al., 2009) as well as the composition of the descending plate (Rüpke et al., 2002). Specifically, the different lithological fluid sources emphasized by different subduction parameters allow for changing fluid addition patterns (mass and fluid-mobile trace element chemistry) down-dip along the subducting plate through the upper mantle. These patterns may directly influence the composition and mass fraction of fluxed melts within the wedge, leading to regional variations in arc lava

* Corresponding author. Fax: +1 301 314 9661.
E-mail address: lhebert@geol.umd.edu (L.B. Hebert).
[1] Present address: University of Maryland, College Park, MD 20742, United States.

0009-2541/$ – see front matter © 2009 Elsevier B.V. All rights reserved.
doi:10.1016/j.chemgeo.2009.06.017

geochemistry. Variations can be compared among different subduction systems, or through cross-arc and along-arc trends within the same subduction system. For example, relative contributions from heterogeneous slab fluid sources can be manifested in diverse chemical characteristics of lavas derived from different depths above the seismic Wadati–Benioff zone (WBZ) (Ryan et al., 1995; Hochstaedter et al., 2001; Stern et al., 2006).

GyPSM-S (*G*eodynamic and *P*etrological *S*ynthesis *M*odel for *S*ubduction) models the dehydration of a subducting slab and the impact of fluid release on the shallow (<200 km) mantle wedge, assuming an equilibrium-based interaction (Hebert et al., 2009). The primary model observation is the development of a water-saturated low-viscosity channel (LVC), which arises due to the partitioning of water into nominally anhydrous minerals (NAM), the thermal structure of the mantle wedge, and the down-dip advection of near-slab material (Hebert et al., 2009). Water in NAM has two consequences: reduction of the peridotite solidus (Mysen and Boettcher, 1975; Gaetani and Grove, 2003; Asimow et al., 2004), and reduction of solid matrix viscosity (Hirth and Kohlstedt, 1996). The thickness of the LVC, which can reach tens of kilometers, separates the slab–wedge interface from the water-saturated peridotite solidus and, hence, melt initiation within the wedge (Hebert et al., 2009). Similar displacements between the slab surface and zones where melt is present within the wedge have been imaged seismically, and have been established by previous geodynamic models (Davies and Stevenson, 1991; Iwamori, 1998; Rüpke et al., 2002, Iwamori, 2007). In GyPSM-S, the locations of melting are strongly determined by the positions of fluid release from dehydration reactions within hydrated slab layers, given a vertical buoyancy-driven fluid migration path (Hebert et al., 2009). The use of the pHMELTS algorithm (Ghiorso and Sack, 1995; Asimow et al., 2004; Smith and Asimow, 2005) in the structure of GyPSM-S allows for predictions of major and trace element compositions of melts and residues and includes a treatment of water (H_2O) as a trace element. However, these compositional predictions are somewhat limited in that pHMELTS cannot yet account for fluid-mobile trace elements carried with the hydrous species from the slab. In order to demonstrate the applicability of GyPSM-S results to regional datasets, additional modeling steps are required to account for the addition of these important fluid-mobile tracers and to make detailed inferences as to the geochemistry of arc lavas with respect to slab fluid sources and as a function of changing subduction parameters. Melt migration processes are neglected in the current formulation of GyPSM-S, which assumes a near-fractional melt extraction scheme and a lack of interaction of extracted melt with the solid matrix (Hebert et al., 2009). However, theoretical treatment of the extracted melts through the established pressure–temperature structure of the wedge is possible. Past studies have suggested mechanisms by which melt generated within the mantle at plate boundaries can transit to the surface. Within the context of convergent boundaries, Spiegelman and McKenzie (1987) describe porous flow driven by pressure gradients as a mechanism of melt focusing towards the wedge corner, Hall and Kincaid (2001) have invoked diapirism of melts towards the overlying lithosphere, and Furukawa (1993) proposes fracture propagation as a mechanism of melt extraction. Kelemen et al. (1997), and references therein, additionally discuss the role of dissolution channels in melt migration at mid-ocean ridges, resulting in a combination of rapid, chemically-isolated melt flow and porous reactive flow.

We use the results of an integrated geochemical and geodynamical study (GyPSM-S, Hebert et al., 2009) of the mantle wedge with regard to fluid source identity, fluid flux, and thermal and hydration structure as a basis for 1-D geochemical modeling of the slab-adjacent wedge. We particularly investigate how slab dehydration patterns change with changing subduction model parameters and how this influences the chemistry of fluid-fluxed melts within the wedge. In addition to a fully-equilibrated pathway of fluid migration, we also consider the consequences of less-interactive fluid paths through the near-slab wedge. Cross-arc and along-arc variations in regional geochemical datasets are compared to the model predictions. Additionally, we offer a discussion of simple melt migration scenarios which may preserve relative heterogeneities in melts initiated at different locations within the wedge.

2. Model parameters and regional significance

The first-order control on the locations of fluid release from the slab (and therefore, the locations of melt production in the mantle wedge) is the slab thermal structure, primarily defined by slab age and secondarily by convergence velocity, such that more mature slabs have significantly different patterns of fluid release than younger slabs (Peacock, 1990; Iwamori, 1998; Hebert et al., 2009, and others). We chose to focus this study on two subduction systems with very different slab thermal structures to more closely examine the potential implications of the different fluid release patterns for melt production and chemistry.

The Northern Izu–Bonin (NIB) intra-oceanic subduction system involves the mature Pacific plate (135 Ma) subducting beneath the Philippine Sea plate at a relatively moderate convergence velocity (~5.0 cm/yr) and a moderate dip angle of 45° (Stern et al., 2003). The arc itself includes a volcanic front, extensional zones, and seamount chains towards the rear-arc trending into the Shikoku Basin (Hochstaedter et al., 2001). The history of the arc involves a multi-stage process (Taylor, 1992; Hochstaedter et al., 2000; Straub, 2003; Bryant et al., 2003). There are two periods of arc formation associated with the IBM system: Eocene–Oligocene volcanism and mid-Miocene to present (Straub, 2003). A hiatus of around 7.5 Ma between these periods (Xu and Wise, 1992) involved rifting associated with the Shikoku Basin (Straub, 2003). The end of the Oligocene marks the end of boninitic lava appearance within the arc record, and the completion of the sub-arc mantle "replacement" stage from an ultra-depleted mantle to depleted Indian MORB-source mantle (Straub, 2003). With resumption of volcanic activity in the mid-Miocene, a quasi-steady-state flow was established within the wedge characterized by (i) continuous advection of Indian MORB-source mantle from the rear-arc that is (ii) continuously fluxed by hydrous slab components, leading to (iii) constancy within temporal trends of major element oxides (Straub, 2003). Straub (2003) therefore suggests that melt formation processes and the source composition are relatively constant in this system and that the thin (~7–22 km) crust does not seem to have a significant impact on lava chemistry. The volcanic front (VF) of the Izu–Bonin arc is one of the most depleted of all volcanic arcs, and there exist significant cross-arc variations in the geochemistry of erupted lavas, including ε_{Nd}, Ba/Nb, U/Nb, and $^{87}Sr/^{86}Sr$ (Hochstaedter et al., 2001). Additionally, there is a lack of evidence of slab-derived sediment melting influence to the shallow (<175 km depth) wedge (Hochstaedter et al., 2001; Plank and Kelley, 2001), which emphasizes the role of slab-derived fluids in the production and geochemistry of mantle wedge melts and makes this system appropriate for modeling by GyPSM-S, which neglects sediment input (Hebert et al., 2009).

The central Costa Rican (CCR) subduction system, on the southeastern end of the Central American arc, involves the subduction of the relatively young Cocos plate beneath the Caribbean plate along the Middle America Trench at moderately fast convergence velocity (~9.0 cm/yr) and a moderate dip angle of 45° (Peacock et al., 2005). The Central American system involves systematic along-arc variations in many geochemical indicators such as $\delta^{18}O$ (Eiler et al., 2005), U/Th, Ba/La, and $Na_{6.0}$. These variations have been linked to geophysical parameters such as slab dip, crustal thickness, and slab composition that vary along arc strike (Carr, 1984; Carr et al., 1990; Rüpke et al., 2002; Abers et al., 2003; Carr et al., 2004). Specifically, it has been concluded that the concentration of trace elements contributed by the slab-derived fluids reaches a minimum beneath the Costa Rican segment (Carr et al., 1990; Leeman et al., 1994; Patino et al., 2000) and

that the degree of melting is relatively lower beneath Costa Rica (Carr et al., 1990). Rüpke et al. (2002) further speculate on the basis of geodynamic modeling that there is a lack of a strong serpentinite-derived fluid release beneath Costa Rica, contributing to the along-arc geochemical differences.

3. Method

3.1. Sampling GyPSM-S results and construction of calculation columns

Hebert et al. (2009) present GyPSM-S results for the thermal structure, locations of slab dehydration, fluid source lithology, and fluid flux for a range of subduction model parameters (e.g. slab age, convergence velocity, slab dip angle), including those approximating the two regional systems of interest (NIB, CCR) (Fig. 1A, B). Within the context of GyPSM-S, compositionally-tagged Lagrangian particles within the slab carry lithological information (Hebert et al., 2009) (Fig. 2A). As the slab descends, the particles advect to higher pressures and temperatures, crossing univariant phase boundaries (Fig. 1C, D) and dehydrate to produce a hydrous fluid (Hebert et al., 2009). The subducting slab (neglecting sediment) is fully hydrated to a depth of 12 km, including 7 km of altered oceanic crust (AOC), and 5 km of serpentinized mantle lithosphere (Hebert et al., 2009). The serpentinization process is hypothesized to occur at the outer rise of subduction zones, where ocean water has the potential to penetrate down large normal faults into the mantle lithosphere, reacting with the lithospheric peridotite to produce hydrous phases such as antigorite and chrysotile (Ranero et al., 2003); however, there remains much speculation as to the depth and degree of lithospheric hydration. For this study, we select a typical GyPSM-S iteration for each model case (representing ~160–280 kyr of subduction).

In order to address the important issue of fluid-mobile tracers that are carried with the hydrous fluid phase, as well as to achieve a more detailed examination of the melting region and the impact of fluid

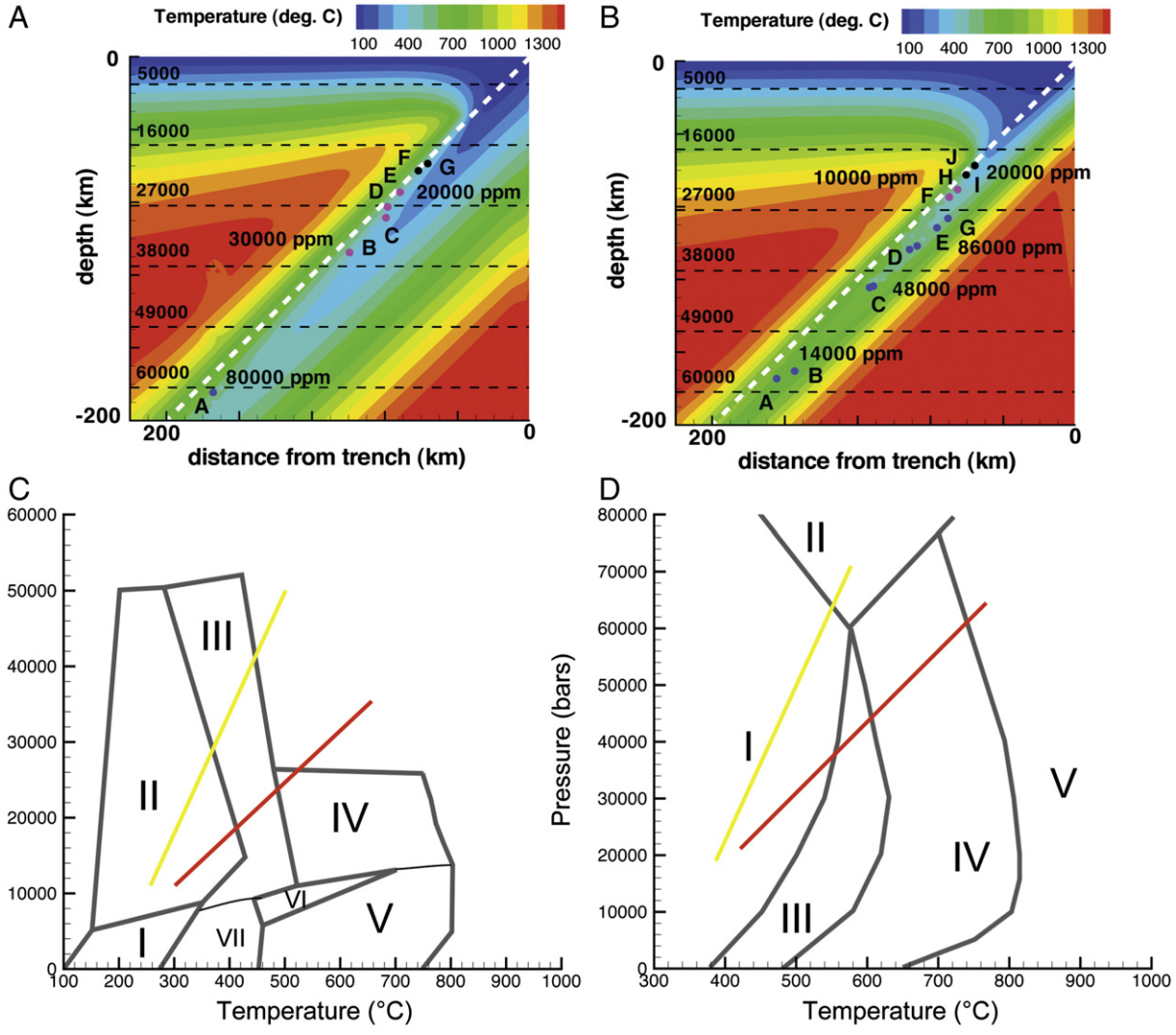

Fig. 1. Results from GyPSM-S calculations showing the thermal structure and example particle fluid release points for models (A) NIB and (B) CCR (Hebert et al., 2009). Fluid mass releases (in ppm) are noted and the dashed white line denotes the slab–wedge interface. AOC dehydration is designated by pink filled circles and lithospheric serpentinite dehydration is designated by blue filled circles. Pressures (in bars) are noted on the left-hand side of the figures and are indicated by horizontal dashed lines. Simplified phase diagrams for MORB (C) and harzburgite (D) from Hacker et al. (2003) with example pressure–temperature trajectories for slab particles from the NIB model case (yellow) and the CCR model case (red). The trajectories for the two models transect different phase boundaries due to the different thermal structures experienced by the slab, respectively. For the MORB case, I: prehnite–pumpellyite facies, containing 4.5 wt.% H_2O; II: lawsonite blueschist, containing 5.0 wt.% H_2O; III: lawsonite amphibole eclogite, containing 3.0 wt.% H_2O; IV: amphibole eclogite, containing 1.0 wt.% H_2O; V: amphibolite, containing 1.3 wt.% H_2O; VI: epidote amphibolite, containing 2.0 wt.% H_2O; VII: greenschist facies, containing 3.0 wt.% H_2O. For the harzburgite case, I: rock containing serpentine chlorite brucite, with 14.8 wt.% H_2O; II: assemblage containing high-pressure hydrous phase A, containing 6.8 wt.% H_2O; III: serpentine chlorite dunite, containing 6.2 wt.% H_2O; IV: chlorite harzburgite, containing 1.4 wt.% H_2O; V: garnet harzburgite, containing 0.0 wt.% H_2O. (For interpretation of the references to colour in this figure legend, the reader is referred to the web version of this article.)

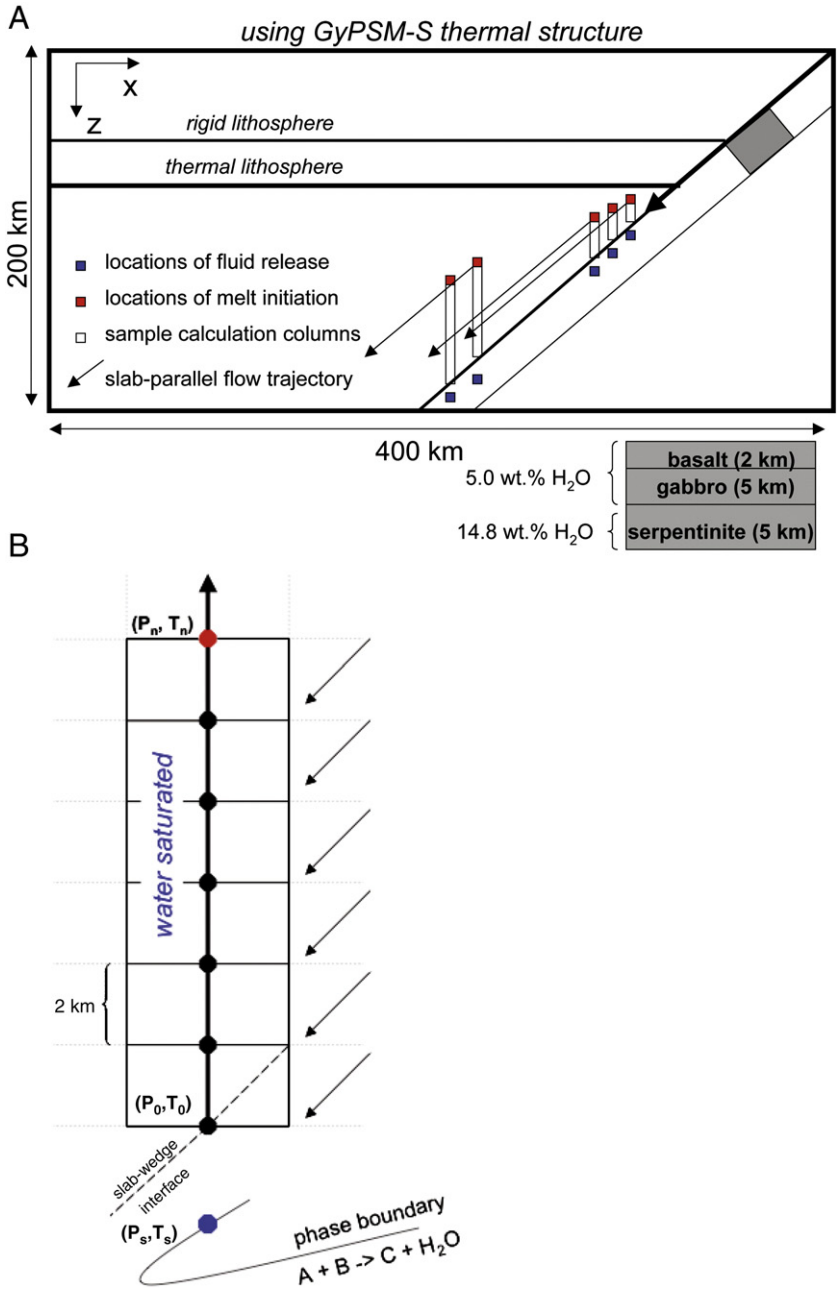

Fig. 2. (A) Schematic view of the GyPSM-S model calculation space (Hebert et al., 2009). Sample columns are shown, as well as approximate locations of fluid release and melt initiation. The layered structure of the subducting crust is detailed in addition to initial water content. (B) Schematic view of a single calculation column showing a phase boundary within the slab and the effective water release point (P_S, T_S) as a dark blue filled circle. The successive equilibration points above the inclined slab–wedge interface are filled black circles labeled (P_0, T_0)…(P_n, T_n), where the final point (red) represents melt initiation where the activity of water drops below unity for the equilibrium assemblage. (For interpretation of the references to colour in this figure legend, the reader is referred to the web version of this article.)

migration, we model one-dimensional geochemical calculation columns (Fig. 2B) through the mantle wedge for the NIB and CCR model cases. Columns originate at the slab–mantle interface immediately above the locations of fluid release, rise through the mantle wedge thermal field, and end where the activity of water in the peridotite drops below unity. If the result of a calculation is water-saturation, the excess fluid moves upwards to the next step (pressure–temperature point). The endpoint corresponds to water undersaturation due to preferential partitioning of water into the melt phase. The columns mimic the dimensional set-up of the GyPSM-S model in that steps between the vertically rising fluid and the wedge peridotite occur in intervals of 2 km along the vertical axis and the pressure and temperature of these equilibration steps are mapped directly from GyPSM-S output on the Eulerian mesh (Hebert et al., 2009). The horizontal extent of the columns is similarly 2 km.

At the start of the column model, the steps along the column have the same bulk composition (DMM, Workman and Hart, 2005). Prior source depletion due to melting at a back-arc or along a decompression trajectory associated with the solid flow is neglected. The columns begin water-saturated up to the respective solidus, which allows the fluid to arrive at the location of melting with negligible loss (loss may be due to stabilization of additional water in NAM as the material advects from lower to higher pressures, due to the increasing solubility of water in NAM with pressure). The first calculation involves the column associated with the lowest-pressure slab fluid release. If melting is present, the bulk composition at that step along

the column is then depleted. This depletion is carried along the flow field to the next column calculation, whereby the residues from the first column calculation become the starting compositions for the second column calculation and so on, assuming advection of the solid down slab-parallel trajectories (Fig. 2A). Calculations to test for melting are performed by individual isothermal, isobaric pHMELTS equilibrations using the Adiabat_1ph user interface (Smith and Asimow, 2005). To reasonable approximation, the mapped GyPSM-S temperature field already accounts for hydration and melting (Hebert et al., 2009). Additional perturbation of the temperature field due to differences between the melting and hydration rates of the column calculation and the original GyPSM-S calculation are neglected.

We consider fluid migration through the near-slab wedge in two ways: (i) assuming that fluid fully equilibrates at each interval with mantle material and (ii) assuming that fluids do not equilibrate with the already hydrated peridotite at each step, but carry the original fluid-mobile trace element composition with them until they reach a point at which melting begins. The difference between these two schemes is manifested within the fluid-mobile trace elements only, and represents two end-member possibilities for fluid transport within the near-slab region. For the full-equilibration sequence, all the columns except the initial (lowest-pressure) column use the fluid-modified trace element composition of the peridotite from the previous column as a starting point to equilibrate with the fluid moving up the current column. For the isolated fluid transport case, the fluid retains its original trace element composition (a function of slab source lithology and initial fluid mass release) until reaching a zone of potential melting. At this point, the fluid-mobile trace element composition is added to the bulk peridotite composition (110 ppm H_2O) that is then equilibrated by pHMELTS. We assume that, in the case of lithospheric serpentinite dehydration, the evolved fluid is isolated from reaction with any overlying crustal layers before starting the column calculation.

3.2. Trace element composition of migrating hydrous fluids (Table 1)

The missing part of the puzzle is the addition of fluid-mobile trace elements, as pHMELTS is sufficient for calculating melt/residue trace element partitioning (including H_2O), but the fluid phase in pHMELTS is pure H_2O with no solute elements. Forward modeling allows calculation of specific fluid-mobile trace elements (Ba, Th, U, Pb, and Sr) based on equilibration of a mass of fluid (the release mass described above) with the slab source lithology (AOC or lithospheric serpentinite) using published partition coefficients, initial concentrations, and the batch melting equation. Of course, the quality of the partition coefficient dataset limits the precision of the models, and the partition coefficients are assumed to remain constant for the respective bulk lithologies over a range of temperatures and pressures, and mineral compositions. We use rock/fluid partition coefficients for fluid in equilibrium with eclogite ($D^{\text{eclogite/fluid}}$) from Brenan et al. (1995) and for fluid in equilibrium with serpentinite ($D^{\text{serpentinite/fluid}}$) from Tenthorey and Hermann (2004). The values for $D^{\text{eclogite/fluid}}$ are calculated assuming a 60:40 garnet: clinopyroxene assemblage. The source chemistry for eclogite is from the altered oceanic crust composition from McCulloch and Gamble (1991). The source chemistry for the serpentinite lithology is the serpentinized peridotite ETF1 (antigorite + olivine + diopside + chlorite + magnetite + Ti-clinohumite) from Erro-Tobbio, Western Alps, NW Italy, analyzed by Scambelluri et al. (2001). Notably, the lithospheric serpentinite composition, compared with the eclogite, is relatively depleted in LILE (Table 1).

For the fully-equilibrated scheme, in each subsequent subsolidus step, we equilibrate the fluid-mobile tracers with a peridotite source lithology based on partition coefficients for fluid in equilibrium with lherzolite ($D^{\text{lherzolite/fluid}}$) (Brenan et al., 1995), assuming 60:30:10 by mass olivine:orthopyroxene:clinopyroxene. The peridotite compositions are carried down from previous columns as described earlier.

Table 1
Partition coefficients and sample column calculation.

Trace elements (fluid-mobile)	Initial ppm serpentinite	Initial ppm AOC	$D^{\text{serpentinite/fluid}}$	$D^{\text{eclogite/fluid}}$	$D^{\text{lherzolite/fluid}}$
Ba	5.7000	26.0000	0.0333	0.0002	7.60E−05
Th	0.0001	0.2700	0.6667	0.4100	0.0890
U	0.0003	0.1400	0.0500	0.5100	0.0250
Pb	0.0500	0.3000	0.0040	0.0100	0.0031
Sr	4.0500	110.0000	0.1000	0.1900	0.0430
Reference	(a)	(b)	(c)	(d)	(e)

Notes: Fluids are assumed to be released in trace element equilibrium from the source lithology (assuming to start with 100.0 g). For example, 0.5 wt.% (0.5 g) fluid fraction released from the AOC layer, using the batch melting equation and the values for $D^{\text{eclogite/fluid}}$ given above, will result in a fluid carrying approximately 4972.41 ppm Ba, 0.65 ppm Th, 0.27 ppm U, 20.07 ppm Pb, and 566.86 ppm Sr.
If this fluid (0.5 g) is then added to 100.0 g of water-saturated subsolidus lherzolite at (P_0, T_0) (Table 1, assuming the composition has not been subject to prior melt depletion), the resulting bulk fluid-mobile trace element composition of the lherzolite + fluid assemblage (100.5 g) will include 25.3 ppm Ba, 0.01 ppm Th, 0.005 ppm U, 0.118 ppm Pb, and 10.46 ppm Sr.
This fluid, after equilibrating with the lherzolite, is then moved along to the next equilibration point (P_1, T_1). Using the batch melting equation and the values for $D^{\text{lherzolite/fluid}}$ given above, the bulk composition of the 0.5 g of fluid equilibrated at (P_0, T_0) and removed to (P_1, T_1) is 4984.61 ppm Ba, 0.107 ppm Th, 0.167 ppm U, 14.60 ppm Pb, and 218.90 ppm Sr.
If this fluid (0.5 g) is then added to 100.0 g of lherzolite at (P_1, T_1), the resulting bulk fluid-mobile trace element composition of the lherzolite + fluid assemblage (100.5 g) will include 25.36 ppm Ba, 0.008 ppm Th, 0.004 ppm U, 0.091 ppm Pb, and 8.72 ppm Sr. This is repeated to (P_{solidus}, T_{solidus}) when the water-saturated solidus is crossed, and melting initiates. At that point, pHMELTS calculates the melt and residue trace element composition based on the lherzolite + fluid bulk composition.

(a) Serpentinite ETF1 from Scambelluri et al. (2001) Supp. Mat.
(b) Altered oceanic crust composition from McCulloch and Gamble (1991).
(c) Tenthorey and Hermann (2004) best estimates of partition coefficients, U and Sr are lower estimates.
(d) Brenan et al. (1995) calculated eclogite/fluid partition coefficients.
(e) Brenan et al. (1995) calculated lherzolite/fluid partition coefficients.

Errors may be introduced due to the changing bulk composition of the peridotite as it melts and is advected, especially as some melting steps lead to exhaustion of clinopyroxene. Prior to a pHMELTS equilibration, the fluid-mobile contents from the fluid (including water as a trace element) are added to the bulk trace element composition of the peridotite, according to the mass proportion of fluid added. After the calculation, any excess water is then given a fluid-mobile trace element content based on its mass fraction and is moved along to the next pressure–temperature point (see Notes to Table 1). Melts calculated at the top of the column thus include the fluid-mobile trace elements added by the hydrous fluid phase. In the isolated transport case for fluid, the fluid interacts with the peridotite source lithology at the top of the column only. Within the GyPSM-S model, fluid is transported using Darcy flow (Hebert et al., 2009). For this study, we necessarily impose that fluid moves fast enough such that it will reach the top of the calculation column before advection would move the solid material in the column to new P–T conditions.

3.3. Melt transport

Realistic melt flow beneath subduction zones is most likely to be at least two-dimensional (Spiegelman and McKenzie, 1987); however, one-dimensional models can provide some insight. In the context of the columns introduced above, we examine the compositions of the melts as they are initiated and address the fate of melts initiated at different depths and distances into the wedge in the context of buoyant transport towards the surface. Vertical transport allows for the least complicated manner of equating melts initiated at different depths to different locations in a cross-arc sense. Two end-member possibilities for melt–solid interaction along this type of trajectory are evaluated.

The fate of the melt can theoretically fit into one of two categories: (i) chemically-isolated transport (perhaps along unreactive channels,

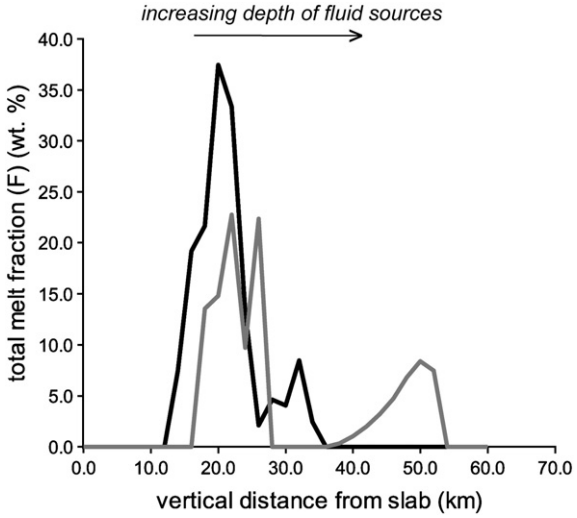

Fig. 3. Plot of total degree of melting (F) experienced by the advecting mantle material at different distances from the slab for CCR (black) and NIB (gray). The maximum melt fractions are extracted from ~15 to 25 km vertical distance from the slab, initiated from mid-pressure fluid releases.

or along fractures) and (ii) reactive transport (porous flow). Both scenarios can be addressed within the column configuration. During the original calculation, described above, information as to the pressure, temperature, composition, and mass fraction of melts generated along a column is provided. However, the original column assumes the transport of water in a hydrous fluid only, and the calculation ends when the activity of water drops below unity. The melting calculation employs an extension of the original column. A single initial melt composition from each original column, representing the maximum melt fraction experienced for that column, is extracted. In the case of isolated transport, we examine the situation in which the melt continues to travel along an extension of its original column, without interaction with the surrounding peridotite. If a calculation results in the persistence of the melt phase, the melt is moved to the next point along the column extension. This is a case of closed system transport, where there is no exchange of mass. In the case of reactive transport, we examine an open system in which the melt continues to move along the column extension, but with equilibration with the surrounding peridotite at each step. In both cases, there is complete physical separation of the melt and residue after each step, such that it is the melt phase alone that moves. For both cases, the extended column calculation continues until the melt fraction drops to zero or the limits of pHMELTS stability are reached.

4. Results

4.1. Dehydration patterns as a function of subduction parameters

Due to the specification of vertical fluid transport through the mantle wedge, the locations of melt initiation are controlled by the positions of the dehydration reactions within the different lithologic layers within the slab. These reactions generate different dehydration patterns in the two models due to the changing thermal structure of the model slabs. In both models, there appears to be a roughly bimodal distribution of fluid sources and an overall evolution in the host reservoir with distance along the slab (Fig. 1A,B). In model CCR, the AOC layer and the serpentinite layer completely dehydrate by the time they exit the base of the model domain (200 km). The AOC layer dehydrates over a pressure range of ~1 GPa before 100 km depth. The serpentinite layer dehydrates in a series of reactions starting at ~3 GPa and ending at ~6 GPa (rock containing serpentine chlorite brucite → serpentine chlorite dunite; serpentine chlorite dunite → chlorite harzburgite; chlorite harzburgite → garnet harzburgite; Fig. 1C, D; lithologic descriptions from Hacker et al., 2003). In model NIB, the AOC layer dehydrates over a longer pressure range (~2 GPa) extending to greater depths. The serpentinite layer crosses a single phase boundary and exits the model domain with 6.8 wt.% H_2O. Increasing the downgoing slab thermal age results in a very strong fluid source from the serpentinite layer at higher pressures (≥5.9 GPa), as opposed to a relatively weak mid-pressure fluid source from the serpentinite layer associated with model CCR. The fluid flux from the slab increases with depth for the model NIB as a function of the capacity of the deeper-dehydrating serpentinite minerals and the position of the phase boundary. For model CCR this is not the case, and the majority of the fluid is released from the interval ~2.5–3.5 GPa. Mid-pressure fluid release (<4.0 GPa) from model CCR is primarily a product of the serpentinite layer, while for model NIB it is the AOC layer. In model CCR, very shallow fluid release results in the hydration of the peridotite wedge without melting, and the fluid continues to migrate up into the overlying lithosphere.

4.2. Melt characteristics

The identity of fluid sources is important for the fluid-mobile trace element chemistry of the resulting melts. As shown in Table 1, the fluid-mobile trace element compositions of the fluids derived from the lithospheric serpentinite are more depleted than those originating from the AOC layer, resulting in different melt trace element signatures depending on the direct fluid source to a specific melting region. Thus, the serpentinite provides a significantly greater fluid source without a corresponding increase in fluid-mobile components, in agreement with Stern et al. (2006). There is a strong control on the initiation of melting with the influx of fluid, and all initial melts at the tops of the columns are very hydrous, with 8–15 wt.% H_2O (higher-pressure initial melts have less water). There is no simple pressure-dependent trend of instantaneous melt fraction (f) of the initial melts that appear in the system. Single columns can produce multiple degrees of f; and in some cases, particularly at shallower melting regions, multiple melts with significantly different concentrations of indicators of source depletion and major element compositions. Overall, initial melts at low- to mid-pressures have higher SiO_2, Al_2O_3, and H_2O and lower TiO_2 contents than higher-pressure melts. Na_2O varies primarily by melt fraction.

The cumulative melt fraction (F) experienced by a packet of mantle within the calculation column as it moves past the base of the model domain changes dramatically between the model with the younger slab and the model with the more mature slab (Fig. 3). Larger fluid flux from the mid-pressure serpentinite fluid releases within model CCR (young slab) result in very high F (>35 wt.%) in the center of the column. For model NIB (mature slab), the maximum F experienced at mid-pressures (associated with a smaller fluid flux from AOC layers) is ~20 wt.%, with a significant tail (up to 10 wt.%) appearing at higher pressures. In both model cases, the activity of water rapidly drops below unity as the water is partitioned into the melt phase. Restricting water transport to a hydrous fluid phase results in a sharp boundary in the water content of NAM and in solid density ($\Delta\rho$~20–50 kg/m^3) between the LVC and the ambient mantle above the melting region. These density contrasts are not enough to initiate Rayleigh–Taylor instabilities leading to diapirism of the hydrated solid (e.g. Gerya and Yuen, 2003); however, the water content boundary leads to strong lateral variations in solid viscosity which have an impact on the flow field as well as geophysical surface observables (Hebert and Gurnis, in press).

4.3. Melt depletion patterns within the wedge

A combination of changing bulk composition due to melting along previous columns, and of the gradual divergence of the pressure–temperature path of the slab surface from the water-saturated solidus, causes the active melting region to occur as a thin lens that appears at a greater distance from the slab interface with increasing depth (Fig. 4).

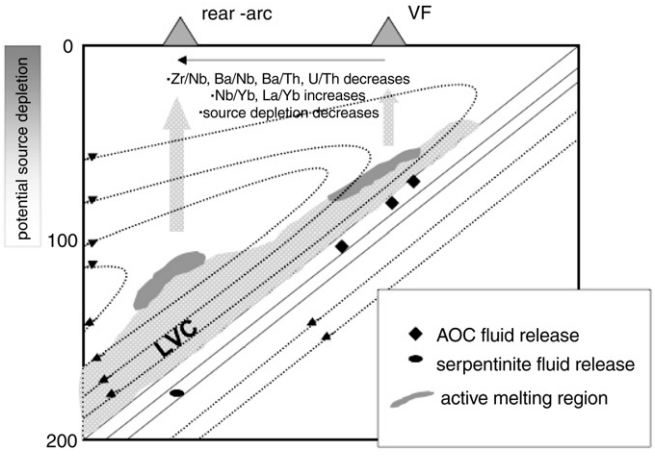

Fig. 4. Cartoon of the LVC, slab fluid releases, and melting regions for an example mature slab model with a moderate slab dip angle. Indicated are potential simple melt migration pathways that would allow deeper melts to impact rear-arc lava chemistry and shallower melts to impact volcanic front (VF) lava chemistry. The trends observed by Hochstaedter et al. (2001) and Stern et al. (2006) for cross-arc variations reflecting distance to WBZ are shown.

We present some of the model data as trace element ratios versus pressure. The *x*-axis (pressure) is a proxy for depth of initial melting, such that model melt compositions that plot at lower pressures are melts initiated as a result of fluid influx from lower-pressure dehydration of fluid sources. Model melt compositions plotted at higher pressures are melts initiated as a result of fluid influx from higher-pressure dehydration of fluid sources. More specifically, we present the pressure as equivalent to a relative "depth to slab" or "distance from trench" measurement. In this way, we can provide a significant link between the composition of the melt and the identity of the slab lithology responsible for the fluid influx resulting in melting. Where applicable, model melts are compared with regional lava datasets.

Incompatible element ratios that reflect source depletion (e.g. Zr/Nb and Nb/Yb) are not significantly affected by the method (isolated versus fully-equilibrated fluid transport) by which fluids transit the hydrated region and show a bimodal distribution correlating with pressure of initial melting. For example, Zr/Nb, which increases with source depletion (Stern et al., 2006), is consistently highest in low- to mid-pressure melting regions in both models (Fig. 5A), where fluid sources are closely spaced. Within low- to mid-pressure region, melts become more depleted with pressure, as residues from previous melting events are advected down-dip and additionally melt. However, these additional melts are generally low melt fraction, and do not result in water undersaturation and fluids will tend to continue on to less-depleted (or non-depleted) sources towards the interior of the wedge, resulting in additional melting with significantly higher melt fractions. Due to progressive depletion at lower pressures and the position of the solidus relative to the slab–wedge interface, mantle residues from the low- to mid-pressure melting region are not the source of high-pressure melts. Overall, we observe a combination of melts produced from fertile mantle sources and melts produced from depleted mantle sources. The most depleted melts are associated with low- to mid-pressure fluid sources: the AOC (eclogite) layer in the case of mature slab model NIB and the serpentinized lithosphere in the case of younger slab model CCR. We also observe that melts associated with deeper fluid releases (from lithospheric serpentinite in both models) are uniformly from more fertile mantle sources.

4.4. Trace element chemistry of model melts

Geochemical tracers carried with slab-derived fluids are affected by the mechanism of fluid transport (fully-equilibrated or isolated) through the hydrated near-slab wedge. Ba shows the most dramatic difference, as its concentration in the fully-equilibrated case rapidly increases within the LVC (a consequence of the low $D^{\text{lherzolite/fluid}}$ for Ba and of the fluid stripping Ba out of an increasing volume of fertile peridotite). Indeed, concentrations of Ba in the peridotite become unrealistic in the fully-equilibrated fluid transport end-member. In contrast, the method of isolated transport of the fluid, (with subsequent isolated transport of melt) results in trace element ratios within the range of regional datasets. The fully-equilibrated fluid path results in enrichments of Pb in the initial melts at all pressures and U and Sr at low- to mid-pressures relative to the limited-interaction fluid path. Th contents in the initial melts are not significantly affected by the choice of fluid transport scheme.

Plots of Zr/Nb versus U/Th (Fig. 5B, C) show the depletion trends together with the degree of hydration. Higher U/Th is expected for mantle sources metasomatized by hydrous fluids, whereas higher Zr/Nb is expected for depleted mantle sources, as mentioned previously. For the younger slab model (CCR) (Fig. 5C), the range of Zr/Nb values of the model data appears to match the regional values reasonably well. The U/Th values of the most of the model dataset fits the regional range, however, there are several points that lie significantly outside the regional data at higher values of U/Th. These points all represent melts fluxed from mid-pressure lithospheric serpentinite-derived fluids and additionally represent melts of previously melt-depleted residues that have advected down-dip. The range of U/Th ratios of the model data of the mature slab model (NIB) data appears somewhat restricted towards lower values compared to the range of regional values represented by the GEOROC dataset for the Izu–Bonin fore-arc/arc. In contrast to the CCR model case, the occurrences of mid-pressure sequential depletion occur associated with fluid flux derived from AOC, and do not result in high (>1.0) values of U/Th. Values for Zr/Nb fail to match the higher end of the GEOROC fore-arc/arc dataset (Zr/Nb>90). This may be due to our DMM starting material composition, or because we have neglected prior melt depletion present in the real system. Overall, melts associated with the majority of model CCR serpentinite fluid release and model NIB AOC fluid release appear to most closely match the regional arc datasets, potentially indicating that the regions of highest melt production (mid-pressure) are most readily represented towards the volcanic front, and that changing subduction parameters can explain the changing fluid source lithology responsible for the mid-pressure fluid release.

The La/Yb ratio represents the mantle source's enrichment in incompatible elements, generally relating to the amount of melting (Rüpke et al., 2002; Stern et al., 2006), and the Ba/La ratio represents the slab-derived fluid's contribution, or the relative slab signal (Rüpke et al., 2002). Plots of La/Yb versus Ba/La (Fig. 5D, E) show that in both models, melts influenced by AOC-derived fluids tend to have lower La/Yb and higher Ba/La. AOC-derived fluid is restricted to the low- to mid-pressure regions, and the previously mentioned melt depletion there explains the lowered La/Yb values. Higher Ba/La can be explained by the higher initial Ba content of the AOC lithology (and, hence, fluid derived from it). It should be noted that the Carr regional dataset (http://www-rci.rutgers.edu/~carr/index.html) for Costa Rica has anomalously high values for La/Yb, derived from Galapagos-like mantle in the area (Leeman et al., 1994; Herrstrom et al., 1995) (Fig. 5D). Our model data do not match the regional dataset because of our use of the DMM model as our initial mantle composition. Model data for NIB appear to capture the overall structure of the La/Yb versus Ba/La regional data distribution (Fig. 5E), with the mid-pressure AOC fluid source represented by GEOROC fore-arc/arc lava regional data trending towards higher Ba/La and lower La/Yb and the high-pressure lithospheric serpentinite source represented by GEOROC rear-arc regional data trending towards lower Ba/La and higher La/Yb.

Some ratios of fluid-mobile incompatible elements to HFSE (generally assumed not to be mobile in fluids), such as Ba/Nb, can be indicative of the total subduction component that is added to the arc magma source (Pearce et al., 2005). Ba/Nb ratios in the models are higher for melts associated with AOC-derived fluid (100–200) and lower

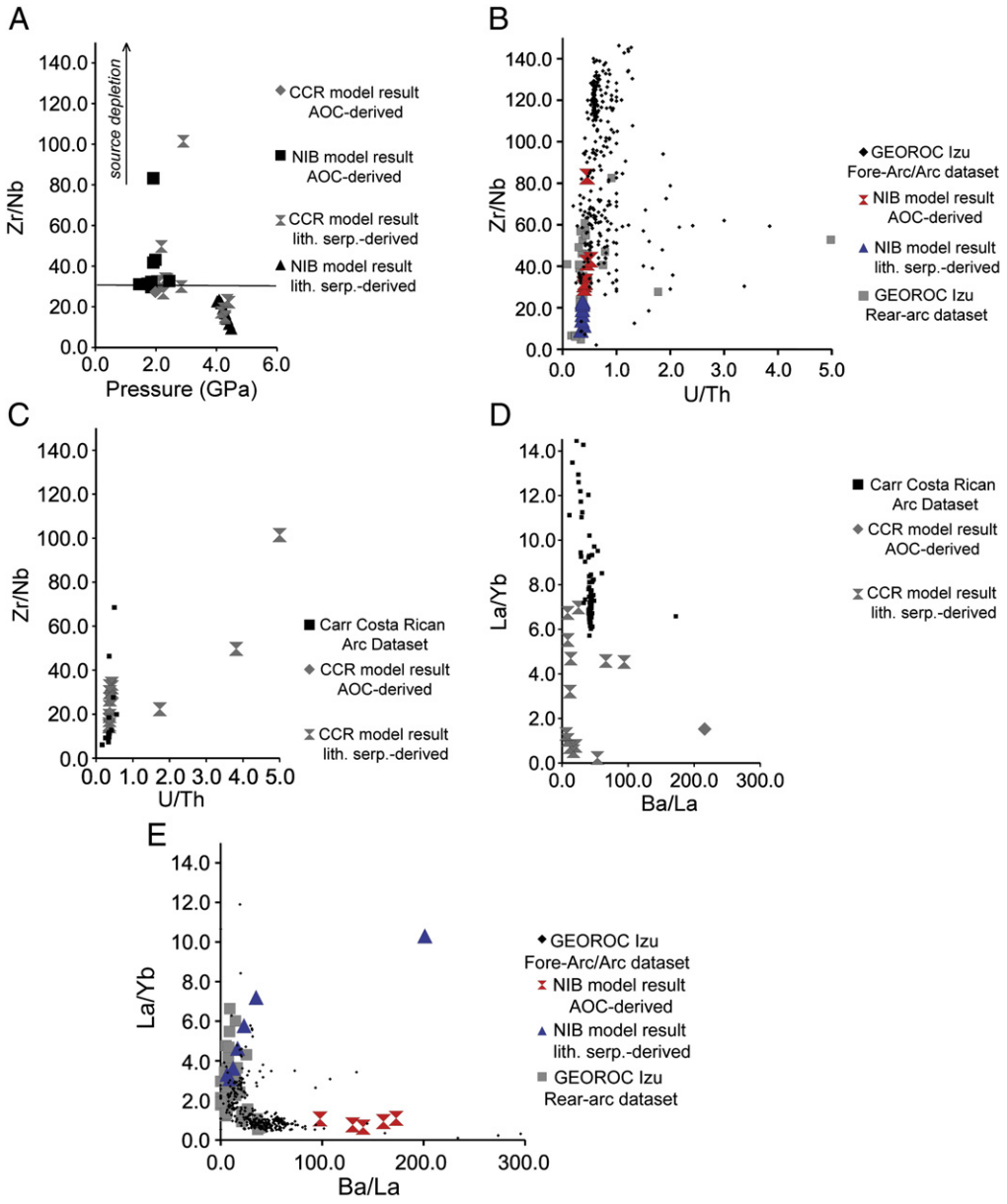

Fig. 5. Plots of modeled trace element ratios for the limited fluid interaction case: (A) indicator of progressive mantle source depletion as a function of slab fluid source lithology and dehydration pressure (MORB value for Zr/Nb ~30 from Stern et al. (2006) indicated by horizontal line); (B, C) degree of mantle source depletion (Zr/Nb) versus indicator of degree of hydration (U/Th) as a function of slab fluid source lithology and compared to regional datasets (NIB: http://georoc.mpch-mainz.gwdg.de/georoc/, dataset covering latitudes 28.5–35°N and longitudes 136–142°E; CCR: http://www-rci.rutgers.edu/~carr/index.html); (D, E) indicators of mantle source enrichment (La/Yb) versus indicators of slab fluid contribution (Ba/La) as a function of slab fluid source lithology and compared to regional datasets.

for melts associated with lithospheric serpentinite (6–150). All model ratios are higher than N-MORB (Ba/Nb~4), reflecting the influence of the slab-related fluid sources (Hofmann, 1988). For the NIB model, Ba/Nb decreases with increasing pressure (Fig. 6A), reflecting a fluid source change from AOC to lithospheric serpentinite. Significantly, NIB model data overlap Ba/Nb data ranges presented by Hochstaedter et al. (2001) for volcanic front (we conclude to be low- to mid-pressure AOC-derived fluid source) and rear-arc (we conclude to be high-pressure serpentinite-derived fluid source) lavas. Plots of Ba/Th and U/Th versus Ba/La (Fig. 6B, C) comparing the Carr dataset with model CCR melts show that the serpentinite-derived fluids from CCR more closely match the majority of the data points from Costa Rica, but in each case, there is an outlier somewhat fit by an AOC-derived point. We infer these relationships to be indicative of low- to mid-pressure fluid releases associated with the volcanic front lavas. In the young slab model (CCR), the source lithology for these fluids is a mixture between AOC at low pressures, and a majority of fluid release from lithospheric serpentinite towards mid-pressures. Plots of Ba/Th and U/Th versus Ba/La (Fig. 6D, E) comparing the Izu–Bonin GEOROC dataset with model NIB melts show a somewhat poorer fit. The range of Ba/Th and Ba/La appears to be captured fairly well by model NIB data, with the higher-pressure fluid release from lithospheric serpentinite associated with melts having similar Ba/Th and Ba/La to the GEOROC rear-arc dataset. However, the U/Th values are too low and the Ba/La ratios are too high for the melts associated with low- to mid-pressure AOC fluid releases to match the fore-arc/arc dataset. This may be due to a homogeneous starting composition for our slab fluid source lithologies, changing partitioning behavior, or, alternatively, this could indicate that the limited-interaction fluid pathway of choice may not be appropriate for U transfer from the slab. A fully-equilibrated pathway provides further

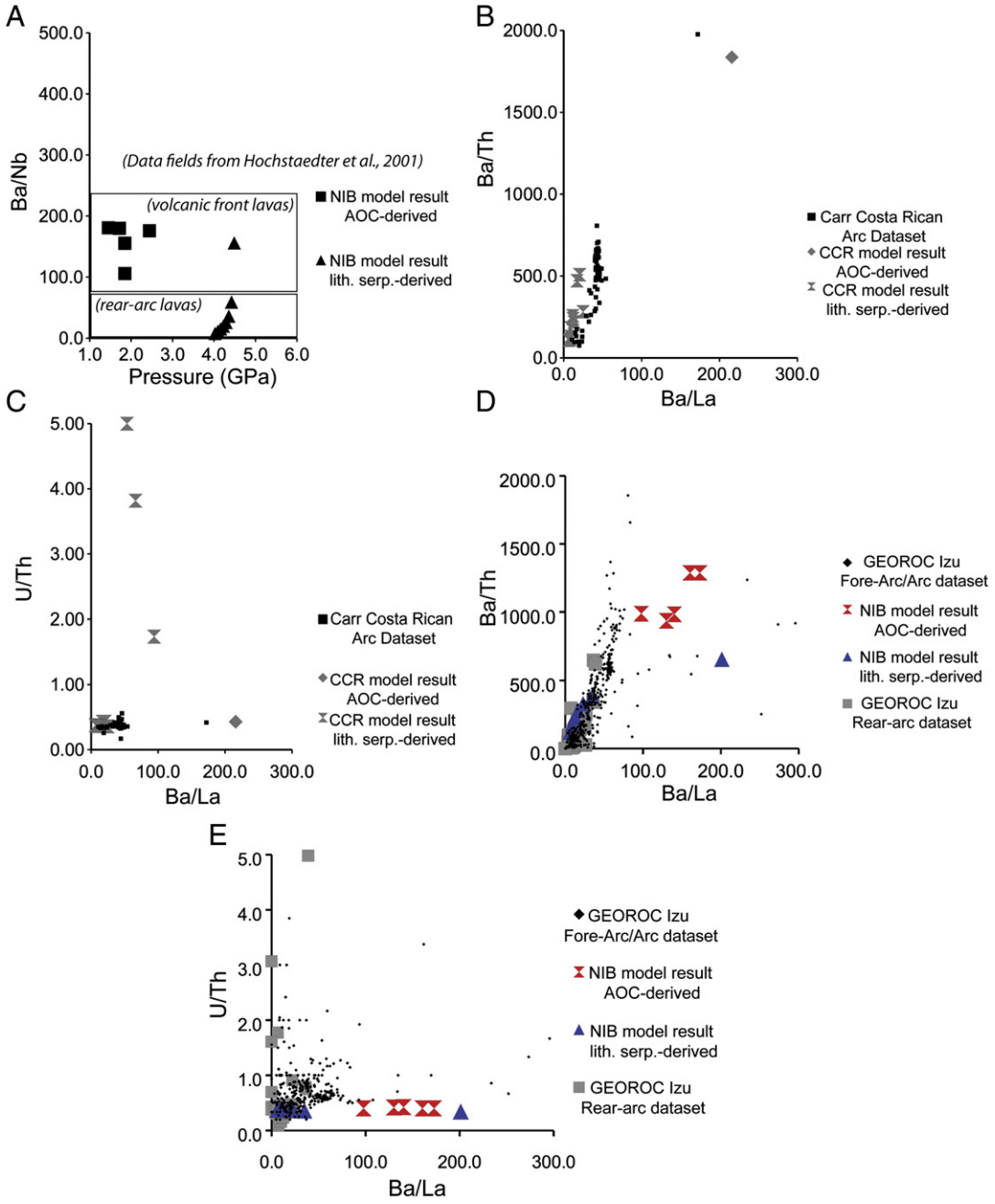

Fig. 6. Plots of modeled trace element ratios for the limited fluid interaction case: (A) ratio of fluid-mobile element to HFSE (Ba/Nb) as a function of dehydration pressure along the slab for NIB model case compared to Ba/Nb data fields from Hochstaedter et al. (2001) for volcanic front and rear-arc lavas, showing that Ba/Nb ratios for model melts associated with mid-pressure fluid releases (AOC) match the volcanic front ratios while the model melts associated with high-pressure fluid release (lithospheric serpentinite) fall in the rear-arc field. (B, D) Ratios of Ba/Th as a function of Ba/La for changing slab fluid source lithology for the CCR and NIB models and (C, E) U/Th as a function of Ba/La for changing slab fluid source lithology for CCR and NIB models compared to regional datasets.

enrichment in U and little variation in Th, which would more closely fit the range of the regional data.

Overall, the fits of our model data to the regional datasets are not conclusive, but considering the necessary simplifications involved in the modeling, we can still make several observations. We note a consistent difference in the fluid-mobile trace element content between melts associated with fluids derived from AOC slab layers and serpentinite slab layers. This reflects the initial composition of the source lithologies, and if undisturbed by fluid transport within the slab, may allow for important conclusions to be drawn about fluid and melt pathways within the wedge. We observe melt depletion trends within the regional datasets that potentially link low- to mid-pressure fluid releases in both model cases with volcanic front lavas. This relationship holds despite changing fluid source lithology between model cases. We note that our model results are potentially significantly affected by a lack of sediment and a uniform initial mantle composition, but that these initial results are nonetheless intriguing for tracing of cross-arc chemical trends related to dehydration of specific slab lithologies.

4.5. Simple models for melt extraction

We attempt two tests of melt extraction: full equilibration and isolated transport of the melt. When melt is fully equilibrated with ambient peridotite at each additional step along the column, two trends

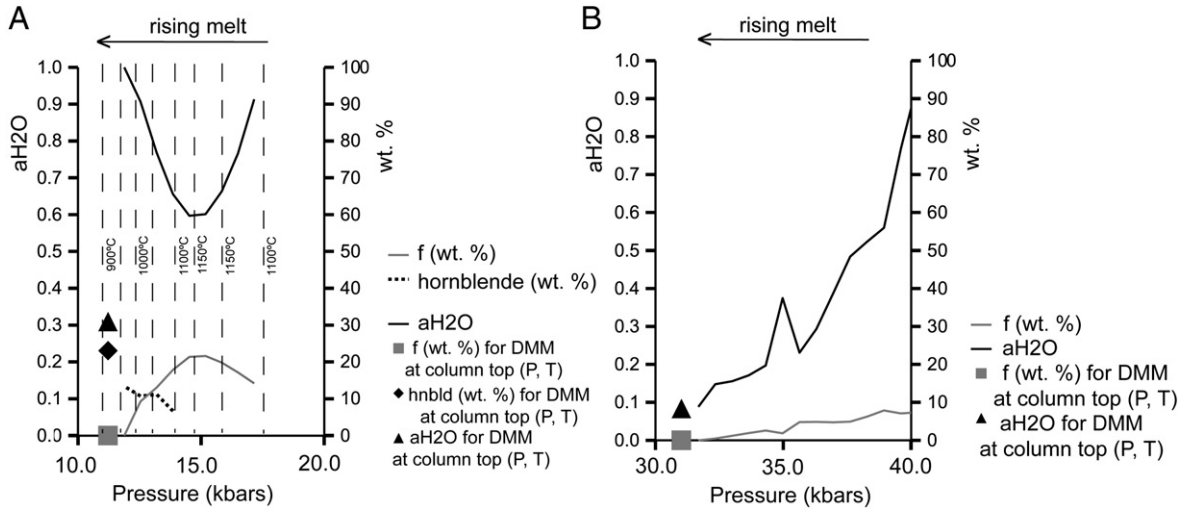

Fig. 7. Results for the simple reactive melt migration case involving full equilibration with the migrating melt and surrounding wedge peridotite along a vertical pressure–temperature path extending above the position of melt initiation. (A) For the case of shallower rising initial melts, the activity of water decreases and then increases, coincident with an increase and then decrease in the overall melt fraction (secondary *y*-axis). Hornblende stability (secondary *y*-axis) corresponds with the decreasing melt fraction. Solid symbols represent values for ambient DMM composition at the pressure–temperature conditions at the top of the reactive column, showing an abrupt jump in the quantities. Vertical dashed lines indicate temperatures within the wedge, with a contour interval of 50 °C, and showing that melt fractions increase to a maximum (~22.0 wt.%) at the apex of the wedge. (B) For the case of deeper rising initial melts, hornblende does not become stable due to the higher pressures (note change in values along the *x*-axis). Also, there is not a jump in quantities at the top of the reactive column with respect to ambient DMM.

emerge. For initial melts that have formed at relatively shallow depths (Fig. 7A), equilibration up the column results in the progressive dehydration of resultant melts and decreasing, then increasing activity of water in the system, with concurrent increases in the water content of NAM in the residues along the column. In this case of reactive flow, melt fraction increases to ~22 wt.%, then decreases as, around 1.35 GPa, the thermal apex of the wedge is reached and hornblende is added to the assemblage. The extended column calculation ends with the activity of water reaching unity (second boiling) and melting ceasing around 1.15 GPa. There is a very abrupt contrast between the conditions at the top of this column and the ambient conditions in terms of water activity and solid density ($a_{H2O} = 1.0$ versus 0.3; $\rho_{solids} = 3.16$ versus 3.28 g/cm^3). For initial melts that have formed at higher pressures (Fig. 7B), the column extension is longer, yet involves lower melt fractions and a steadily decreasing melt phase. Hornblende stability is never reached, due to the higher pressures. Instead, water is progressively partitioned into the residual NAM, with water activity and solid density decreasing to ambient levels ($a_{H2O} = 0.08$; $\rho_{solids} = 3.27$ g/cm^3). Interestingly, the situation of complete melt equilibration along a vertical path results in an extension of the hydrated layer (defined by higher concentrations of water in NAM than ambient DMM) beyond the original thickness of the LVC. Reactive flow of the hydrous melt within the wedge may lead to a greater extent of spatial viscosity reduction than proposed by Hebert et al. (2009). For the case of isolated transport of melt along the pressure–temperature path specified by an extension of the original column, second boiling occurs at relatively greater depths (~1.25 GPa).

5. Discussion

5.1. Fluid transport within the LVC

Fluid transport modeling with the assumption of full equilibration of the fluid with peridotite along the entire thickness of the LVC is not matched by the fluid-mobile trace element datasets for either region except, perhaps, with regard to U. In fact, it is the assumption of equilibration of the fluid with peridotite only at the top of the transport pathway that appears to be more valid. These end-member results could be indicative of limited interaction of the fluids with the hydrated peridotite along the pathway, not necessarily only near the melting region. As the LVC is initiated near the wedge corner, at the shallowest locations of fluid release, and water in NAM is quite stable within the LVC throughout its transit to (at least) the base of the model domain (200 km depth), the primary impact of the equilibration of fluid is to increase the water content, and perhaps thicken the LVC. A more limited interaction will not negate the presence or persistence of the LVC, and will act to more readily preserve the differences in fluid-mobile trace element chemistry derived from particular source lithologies along the slab, leading to discernible influences on the initial melt chemistry that vary spatially within the wedge. If these differences are preserved, and a melt migration scheme acts to prevent significant mixing of magmas within the wedge, such that melts associated with higher-pressure-derived slab fluids will erupt separately from melts associated with lower-pressure-derived slab fluids, cross-arc variations in lava trace element chemistry become significant for depth tracing of initial melts.

The concept of a changing fluid source slab lithology manifested in rear-arc to arc geochemical trajectories has been proposed by previous studies (Hochstaedter et al., 2001; Stern et al., 2006). The Guguan cross-arc chain represents the fluid-fluxed end-member of the intra-oceanic Mariana arc and involves subduction of a mature slab (Elliott et al., 1997; Woodhead et al., 2001). Stern et al. (2006) propose that changing slab sources of metasomatic fluids with depth lead to variations in the fluid-mobile trace element concentrations in the lavas in this system (Fig. 4), concluding that there may be an increasing role of serpentinite-derived fluids at greater depths leading to rear-arc volcanism with a weakening slab signature with increasing height above the WBZ. As hypothesized by Stern et al. (2006), this could simply be due to the relatively lack of LILE in subducting serpentinized lithosphere. Notably, the water contents of rear-arc lavas are not shown to change markedly from volcanic front lavas, further suggesting a changing slab fluid source to serpentinite, which provides a significant fluid flux (Stern et al., 2006). If the fluid source-derived geochemical differences are preserved, changing subduction parameters (such as slab dip) may produce changing lava geochemistry, as different fluid sources are emphasized (Fig. 1). For example, volcanic front lavas along the Central American subduction system demonstrate that trace element data may preserve information about the relative influences of fluid source lithology as ratios associated

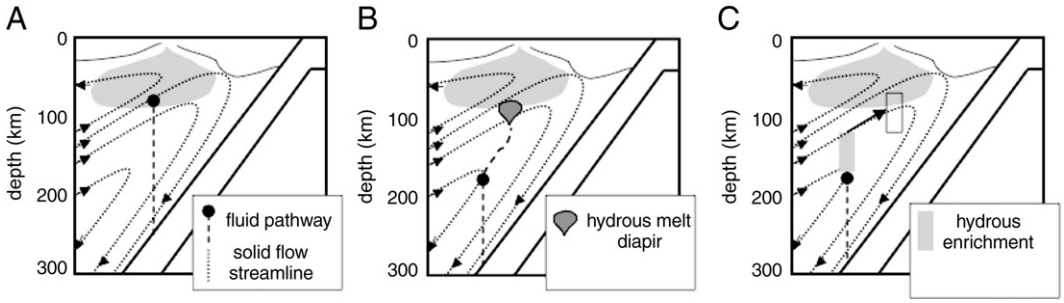

Fig. 8. Schematic models for transport of fluids and/or melts to the back-arc melting region: (A) in this model, which is similar to the ultimate development of the mature slab system (Hebert et al., 2009), continuous fluxing of the deep melt region by a strong serpentinite-derived fluid source results in progressive lengthening of the fluid pathway such that low-pressure, hydrous melts can be generated by direct delivery of fluids to the base of the BABB melting region. (B) Diapiric rise of hydrous melts generated at depth transport material to the base of the BABB melting region. (C) Melt transport along a vertical path beyond the water-saturated solidus results in a freezing of the melt into an enriched mantle packet, which is transported along solid streamlines to the base of the BABB melting region.

with a slab signal vary with respect to changing subduction parameters (Rüpke et al., 2002).

Chlorite is stabilized along much of the slab surface within the LVC in a thin layer (~10 km) (Smith et al., 2007; Hebert et al., 2009). As the slab subducts, the chlorite layer breaks down ~5 GPa, leaving the NAM as the major slab-adjacent water reservoir as subduction continues towards the transition zone (Hebert et al., 2009). We suggest that fluids transit the LVC with little modification along the water-saturated peridotite pathway. However, there is the possibility that hydrous phases present along the slab surface may act as additional trace element 'filters'. There is some evidence for shifts in lava chemistry in the southern Kamchatkan subduction zone that may correspond to the cross-arc limit of chlorite stability at depth (S. Duggen, personal communication), indicating that a stable layer of chlorite within the wedge may affect trace element composition of fluxing fluids.

This study neglects sediment-derived fluid contributions to the fluid budget, as well as sediment melts, or melts of the AOC (Kelemen et al., 2003). We assume that sediment-derived fluids are expelled at shallower depths than the convecting mantle wedge (Rüpke et al., 2002), but the lack of sediment melting may be significant. At present, modeling of slab-derived components encompasses selected fluid-mobile trace elements only. Melting of sediment allows for the bulk addition of elements concentrated in the sediment layer to the mantle wedge that may not be effectively added through fluid-dominated transport alone, due to the very low mobility of certain elements within a fluid. These elements include the HFSE (Nb, Ta, Zr, and Hf), REE, and possibly Th (Brenan et al., 1995; Keppler, 1996; Elliott et al., 1997). Neglecting sediment melting effectively results in the potential for higher concentrations of these elements than predicted by this study.

5.2. Comparison of model results with regional datasets

5.2.1. Costa Rica (CCR)

Rüpke et al. (2002) use a 2-D dynamic model to track the evolving sources of fluid release from the downgoing slab in the Costa Rican subduction zone. The results show that sediments dewater by 75% during shallow (<50 km) subduction, the AOC (the most significant source of the slab-derived fluid flux) dewaters over an interval of 100–140 km depth, and serpentinites dewater over an interval of 130–150 km depth. Our results show a similar overlap between AOC and serpentinite dehydration, but that serpentinite is the major source of mid-pressure (80–130 km depth) fluid flux. Significantly, the fluid sources for the CCR model in this study and the model of (Rüpke et al., 2002), despite the fundamental difference in fluid source lithology, feed into similar spatial melting regions. These mid-pressure melts represent the result of the highest fluid flux in the CCR model, as well as the highest melt fraction, and can thus be considered to be the primary input towards the volcanic front. Lithospheric serpentinite is relatively depleted in fluid-mobile elements compared to subducting AOC. The reason the concentration of trace elements added to the melting region from the dehydrating slab decreases beneath Costa Rica as opposed to neighboring regions with different subduction parameters (Carr et al., 1990; Leeman et al., 1994; Patino et al., 2000; Rüpke et al., 2002) may be this change in fluid source lithology. The range of melting expected beneath Costa Rica is 5–25% (Carr et al., 1990), which is significantly lower than the maximum degree of melting produced by the column modeling of this study, but is not inconsistent with the overall range of melting produced by the columns (Fig. 3). The upper value is probably a consequence of a maximum fluid flux to the active melting region in the column modeling.

Carr et al. (2007) argue that regional along-arc variation in Ba/La in the Central American subduction system is a result of the manner of fluid delivery and its impact on melt production. Specifically, Carr et al. (2007) contend that the steeper-dipping, slightly older slab beneath the Nicaraguan segment involves more concentrated fluid delivery, leading to higher Ba/La, while more diffuse fluid introduction in Costa Rica, a function of the more moderately-dipping slab, leads to lower Ba/La ratios. Models of steeply dipping slabs using GyPSM-S provide evidence for a more concentrated fluid flux at mid-pressure regions feeding the volcanic front (Hebert et al., 2009). Specifically, fluids from greater depths along steeply dipping slabs move along pathways that approach the same melting region as shallow fluids. However, an additional factor for consideration may be the fluid source lithology. Fluids derived from the slab AOC layer tend to result in melts with higher Ba/La ratios, while fluids derived from the slab serpentinized lithospheric layer tend to result in melts with lower Ba/La. Perhaps there is a change from mid-pressure AOC-derived fluid flux under Nicaragua to mid-pressure serpentinite-derived flux beneath Costa Rica, a function of the slightly different slab age. This would not preclude the arguments of Eiler et al. (2005), which lead to the conclusion that there is a strong slab-derived fluid source designated by a low-$\delta^{18}O$ water-rich component beneath Nicaragua. We suggest that it is the deeper AOC layers that would be dehydrating at the mid-pressure ranges in the older slab, and hydrothermally-altered lower oceanic crust and hydrothermally-altered ultramafic rocks both have similar ranges for oxygen isotope values ($\delta^{18}O_{SMOW} = 0$–6‰) (Magaritz and Taylor, 1974; Alt et al., 1986; Staudigel et al., 1995).

5.2.2. Izu–Bonin

Izu–Bonin arc tephra geochemistry indicates minimal contribution from subducted sediment, a dominantly fluid-based slab-component transport scheme, and a highly depleted mantle source for the volcanic arc (Bryant et al., 2003). Additionally, there is a cross-arc distribution of chemical characteristics that indicates that the melt transport systematics can be described relatively simply (Hochstaedter et al., 2001) and shows evidence for a lack of crustal contamination (Straub, 2003). We propose that there is a maximum contribution at the volcanic front from primary magmas fluxed by mid-pressure fluid release from dehydrating

slab AOC layers and that rear-arc lavas (Western Seamounts) involve significant contributions from primary magmas fluxed by fluids released at higher pressures from the dehydrating slab serpentinite layer.

Hochstaedter et al. (2001) note significant cross-arc trends for the Izu–Bonin system, including increasing Nb/Zr (decreasing mantle source depletion) and decreasing Ba/Nb and SiO_2 with distance from the volcanic front to the rear-arc. These trends agree with the results of this study, assuming a melt migration pathway allowing melts initiated by fluids released at lower pressures to influence the volcanic front, and melts initiated by fluids released at higher pressure to influence the rear-arc. Specifically, with regard to the end-member results for limited fluid interaction, the values for Ba/Nb for the low- to mid-pressure melts and the higher-pressure melts match closely the data from Hochstaedter et al. (2001), for volcanic front lavas and rear-arc lavas, respectively (Fig. 6A). Additionally, we observe a trend of decreasing SiO_2 with increasing pressure among initial modeled melts, and trace element indicators of mantle source depletion show that melts associated with low- to mid-pressures are the most depleted in HFSE, a pattern that matches the data from Hochstaedter et al. (2001) indicating that the volcanic front lavas are the most depleted of the arc system (Fig. 5A). Stern et al. (2006) additionally observe increasing mantle source depletion with decreasing height above the WBZ.

In subduction systems there is the potential for sequential melting of mantle peridotite as it advects along streamlines within the wedge, including upwelling beneath a back-arc, melting beneath rear-arc volcanoes, and further melting beneath the magmatic front itself (McCulloch and Gamble, 1991; Woodhead et al., 1993; Hochstaedter et al., 2001; Stern et al., 2006). However, in this study, previous depletions due to such factors are neglected, and depletion trends in the trace elements can be observed solely as a consequence of proximity of fluid sources in the low- to mid-pressure regions, leading to certain cases of additional fluxing of material previously depleted by melting. This is particularly appropriate for the NIB system, which has very depleted arc lavas, yet no active back-arc spreading (Hochstaedter et al., 2000). As demonstrated by the results presented here, and as suggested by Taylor and Martinez (2003), hydrous fluxing alone may maintain the depletion of arc sources. Even if the presence of a back-arc is considered, the solid flow pattern is such that more wedge-interior streamlines may not have passed through melting regions feeding the back-arc melting region, leading to a general trend of melts from less-depleted sources associated with deeper fluid releases (Fig. 4). This leads to an interesting, perhaps ironic, observation: the most fertile mantle sources receive the most fluid-mobile trace element depleted slab-derived fluids. Hochstaedter et al. (2001) propose that a mechanism of fluid depletion can explain the cross-arc melt depletion trend, such that a "fertile" (higher in fluid-mobile elements) slab fluid is released at lower pressures, and a then more "depleted" slab fluid (a result of the earlier fluid release) is released at higher pressures. We suggest that instead of a progressively-dehydrating singular slab source that evolves with regard to concentrations of fluid-mobile elements, there is a condition of progressive dehydration from heterogeneous slab lithologies defined by different initial fluid-mobile trace element compositions and varying fluid fluxes, a situation similar to that modeled by Rüpke et al. (2002) and suggested by Stern et al. (2006).

5.3. End-member results for vertical melt transport

There is a close spatial agreement with the GyPSM-S modeled locations of melt initiation (Hebert et al., 2009) and seismic imaging results for low-velocity zones within the wedge (Zhao, 2001; Hasegawa et al., 2005; Nakajima et al., 2005), indicating that models of the active melting region are successful. However, in order to preserve the spatial heterogeneity of initial melts as described in previous studies of cross-arc geochemistry, a nearly-vertical melt migration model is required. This model should readily allow the arrival of melts fluxed by fluids derived from lower pressures towards the arc front versus melts fluxed by fluids derived from higher pressures towards the rear-arc. The rear-arc lavas in the Guguan chain show higher pressures and temperature of equilibration (Stern et al., 2006), an indication that deeper melts may tend to influence volcanism towards the rear of the arc as opposed to the volcanic front itself. There also appear to be lower degrees of melting experienced as depth to the WBZ increases in the Guguan chain (Stern et al., 2006) (shown from variations in alkali content), a similar result to the column modeling, where deeper melting of less-depleted sources results in lower melt fractions (Fig. 3).

This study involves the investigation of two end-member interaction scenarios accompanying vertical melt transport from the zone of active melting upwards through the mantle wedge. A scenario in which melts remain isolated from the surrounding peridotite matrix results in a short additional transit of the melt before it results in second boiling. In the case of full equilibration with ambient peridotite at each step (Fig. 7), water may be added to NAM from melts migrating beyond the limit of free fluid migration, providing a potential mechanism to generate a more expansive low-viscosity geometry. This mechanism could potentially explain the development of the low-viscosity "wedge" geometry as parameterized by Billen and Gurnis (2001). Melts continue to react along the column to the point of freezing out (higher pressure) or stabilizing hornblende (lower-pressure). Because melts have to approach the surface in order to result in arc lavas, an infinitely permeable scenario can only work for part of the transport process (<40 km depth), and only for shallower melts. The deepest melts in the models may end up as source enriching agents rather than coherent melts passing through the long potential melting column to eruption. In both end-member cases, the column calculation ends well before the depth of potential shallow magma chambers feeding the arc, resulting in the conclusion that neither of these interaction mechanisms by itself defines the entire melt extraction pathway.

5.4. Implications for slab-component transport rates

The stability of the slab-adjacent hydrated zone (LVC) and the separation of the slab–wedge interface from the melting region have been established through GyPSM-S modeling (Hebert et al., 2009). Studies of slab fluid component transport to the arc using U-series isotopes indicate a timeframe of transport from fluid release to eruption between 30 000 and 120 000 years, allowing for a fluid transport rate of 1–4 m/yr (Hawkesworth et al., 1997), and implying the probability of a rapid transport pathway. From comparison with regional datasets, the results presented in this study indicate that fluids responsible for flux melting may preserve the trace element signatures of the original dehydrating lithology with little modification along their pathway through the LVC to the melting region. This suggests either a potential rapid transport scenario that prevents significant fluid–mantle interaction or a fluid-dominated trace element budget. Perhaps hydraulic fracture plays a subordinate role in the slab–adjacent mantle wedge, allowing for a more or less direct delivery of fluid to melting region (Davies and Rowland, 1997).

5.5. Implications for back-arc basin basalt (BABB) sources

There is a critical role of water, originating presumably at the slab–wedge interface, evident in the petrogenesis of basalts erupted at back-arc basins (Stolper and Newman, 1994; Taylor and Martinez, 2003; Kelley et al., 2006). However, the pathways of water delivery from the slab to the back-arc melting region have not been clearly established. In this study, we do not include a back-arc spreading region and cannot therefore offer a unique solution. Despite this, we can infer potential hydrous pathways leading to melting beneath the back-arc from the results presented here.

One published investigation of BABB geochemistry invokes mixing between dry, fractional melts from depth and hydrous melts that have been equilibrated at low pressures (Langmuir et al., 2006). The hydrous end-member is associated with fluid influx from the slab, and requires low-pressure equilibration in order to explain aspects of the geochemistry of BABBs such as low $Fe_{8.0}$ and the lack of a garnet signature (Langmuir et al., 2006).

The model domain in GyPSM-S extends to 200 km depth (Hebert et al., 2009), and dehydration reactions within the slab over that depth range lead to active melting that can explain trace element variations evident in cross-arc lavas. Rüpke et al. (2004) hypothesize that serpentinite dehydration reactions within the slab, and possibly within the hydrated near-slab mantle, can occur at even greater depths, allowing for melting to initiate further inboard from the arc, perhaps extending beneath a back-arc. These deep sources may promote cooling of the wedge, upward retreat of the water-saturated solidus, and, eventually, formation of long, serpentinite-derived fluid pathways to shallower melting regions beneath the back-arc, similar to the mature slab GyPSM-S results (Hebert et al., 2009). This could potentially translate into low-pressure hydrous melting beneath the back-arc as required by Langmuir et al. (2006) (Fig. 8A).

Even if fluid pathways did not reach directly into the BABB source region, fluids generated by deep serpentinite dehydration result in hydrous melting further into the mantle wedge than at shallower areas, removing the active melting region farther from the down-dip influence of the slab-parallel solid flow field. The density differences between the initial melts and solid residue are significant ($\Delta\rho = 400$–$500\ kg/m^3$), and could result in buoyant transport of hydrous melts as diapirs vertically into the BABB source region, as suggested by Langmuir et al. (2006) (Fig. 8B).

Porous flow of relatively low-degree melts at depth may result in an extension of wedge hydration above the zone of fluid delivery to the active melting region. The concentrations of water in NAM are increased in the solid residue due to equilibration with the migrating hydrous melt. Ultimately, the melt will freeze out in this process, but the remaining solid along its migration path may then be carried as hydrous enrichments with the flow field towards the back-arc source region (Fig. 8C).

6. Conclusions

This study involves a supplement to original GyPSM-S modeling of systems with varying subduction parameters in order to demonstrate the applicability of GyPSM-S results to regional geochemical datasets. Changing patterns of fluid release from dehydration reactions within slab lithologic layers as a function of distance down-dip along the slab were investigated and related to the influence of changing parameters such as slab age and convergence velocity. Modeling of fluid migration through hydrated peridotite within the LVC provides evidence for a limited fluid–rock interaction, preserving the fluid-mobile trace element chemistry associated with the original slab lithology to the active melting region. This suggests the potential for either a rapid fluid transport scenario or a fluid-dominated trace element budget within the LVC. Comparison with interpretations of along-arc trends suggests that changing subduction parameters significantly affect the dehydration pattern within the subducting slab, leading to changes in reaction location within the slab and a varying fluid flux and fluid chemistry reaching the active melting region, which can be manifested in erupted lavas. By comparison with regional datasets and interpretations of cross-arc and along-arc trends, we find that a simple melt migration scheme which preserves spatial heterogeneity of initial melts towards eruption is likely. Specifically, that melts associated with low- to mid-pressure fluid release will erupt towards the volcanic front and melts associated with higher-pressure fluid release will erupt towards the rear-arc. Although we do not explicitly include a back-arc in these models, interpretations of the results lead to several potential mechanisms to explain hydrous inputs to back-arc source regions.

Acknowledgments

The authors would like to thank C. Hall and M. Gurnis for collaboration in the GyPSM-S modeling effort. We additionally thank editors Paul Hall, Stephanie Escrig and D.B. Dingwell. Very helpful reviews were provided by James Conder and an anonymous reviewer. Support was provided through the Tectonics Observatory by the Gordon and Betty Moore Foundation.

References

Abers, G.A., Plank, T., Hacker, B.R., 2003. The wet Nicaraguan slab. Geophysical Research Letters 30 (2), 1098 http://dx.doi.org/10.1029/2002GL015649.
Alt, J.C., Muelenbachs, K., Honnorez, J., 1986. An oxygen isotopic profile through the upper kilometer of the oceanic crust, DSDP hole 504B. Earth and Planetary Science Letters 80, 217–229.
Arculus, R.J., 1994. Aspects of magma genesis in arcs. Lithos 33, 189–208.
Asimow, P.D., Dixon, J.E., Langmuir, C.H., 2004. A hydrous melting and fractionation model for mid-ocean ridge basalts: application to the Mid-Atlantic Ridge near the Azores. Geochemistry, Geophysics, Geosystems 5 (1), Q01E16. doi:10.1029/2003GC000568.
Billen, M.I., Gurnis, M., 2001. A low-viscosity wedge in subduction zones. Earth and Planetary Science Letters 193, 227–236.
Brenan, J.M., Shaw, H.F., Ryerson, F.J., Phinney, D.L., 1995. Mineral–aqueous fluid partitioning of trace elements at 900 °C and 2.0 GPa: constraints on the trace element chemistry of mantle and deep crustal fluids. Geochimica et Cosmochimica Acta 59 (16), 3331–3350.
Bryant, C.J., Arculus, R.J., Eggins, S.M., 2003. The geochemical evolution of the Izu–Bonin arc system: a perspective from tephras recovered by deep-sea drilling. Geochemistry, Geophysics, Geosystems 4 (11), 1094. doi:10.1029/2002GC000427.
Carr, M.J., 1984. Symmetrical and segmented variation of physical and geochemical characteristics of the Central American volcanic front. Journal of Volcanology and Geothermal Research 20, 231–252.
Carr, M.J., Feigenson, M.D., Bennett, E.A., 1990. Incompatible elements and isotopic evidence for the tectonic control of source mixing and melt extraction along the Central American arc. Contributions to Mineralogy and Petrology 105, 369–380.
Carr, M.J., Feigenson, M.D., Patino, L.C., Walker, J.A., 2004. Volcanism and geochemistry in Central America: progress and problems. Geophysical Monograph 138, 153–174.
Carr, M.J., Saginor, I., Alvarado, G.E., Bolge, L.L., Lindsay, F.N., Milidakis, K., Turin, B.D., Feigenson, M.D., Swisher III, C.C., 2007. Element fluxes from the volcanic front of Nicaragua and Costa Rica. Geochemistry, Geophysics, Geosystems 8 (6). doi:10.1029/2006GC001396.
Davies, J.H., Rowland, A., 1997. Importance of temperature-dependent viscosity and hydraulic fracture on physical models of subduction zone magmatism. Geological Society of Australia Abstracts 45, 17–20.
Davies, J.H., Stevenson, D.J., 1991. Physical model of source region of subduction zone volcanics. Journal of Geophysical Research 97 (B2), 2037–2070.
Eiler, J.M., Carr, M.J., Reagan, M.K., Stolper, E., 2005. Oxygen isotope constraints on the sources of Central American arc lavas. Geochemistry, Geophysics, Geosystems 6 (7), Q07007. doi:10.1029/2004GC000804.
Elliott, T., Plank, T., Zindler, A., White, W., Bourdon, B., 1997. Element transport from slab to volcanic front at the Mariana arc. Journal of Geophysical Research 102 (B7), 14991–15019.
Furukawa, F., 1993. Magmatic processes under arcs and formation of the volcanic front. Journal of Geophysical Research 98, 8309–8319.
Gaetani, G.A., Grove, T.L., 1998. The influence of water on melting of mantle peridotite. Contributions to Mineralogy and Petrology 131 (4), 323–346.
Gaetani, G.A., Grove, T.L., 2003. Experimental constraints on melt generation in the mantle wedge. Geophysical Monograph 138, 107–134.
Gerya, T.V., Yuen, D.A., 2003. Rayleigh–Taylor instabilities from hydration and melting propel 'cold plumes' at subduction zones. Earth and Planetary Science Letters 212, 47–62.
Ghiorso, M.S., Sack, R.O., 1995. Chemical mass transfer in magmatic processes; IV, a revised and internally-consistent thermodynamic model for the interpolation and extrapolation of liquid–solid equilibrium magmatic systems at elevated temperatures and pressures. Contributions to Mineralogy and Petrology 119 (2–3), 197–212.
Hacker, B.R., Abers, G.A., Peacock, S.M., 2003. Subduction factory-1. Theoretical mineralogy, densities, seismic wave speeds, and H_2O contents. Journal of Geophysical Research-Solid Earth 108 (B1) http://dx.doi.org/10.1029/2001JB001129.
Hall, P., Kincaid, C., 2001. Diapiric flow at subduction zones: a recipe for rapid transport. Science 292, 2472–2475.
Hasegawa, A., Zhao, D.P., Hori, S., Yamamoto, A., Horiuchi, S., 2005. Deep structure of the northeastern Japan arc and its implications for crustal deformation and shallow seismic activity. Tectonophysics 403, 59–75.
Hawkesworth, C.J., Turner, S.P., McDermott, F., Peate, D.W., Calsternen, P., 1997. U–Th isotopes in arc magmas: implications for element transfer from the subducted crust. Science 276, 551–555.
Hebert, L.B., Gurnis, M., in press. Geophysical implications of Izu–Bonin mantle wedge hydration from chemical geodynamic modeling. Island Arc.

Hebert, L.B., Antoshechkina, P., Asimow, P., Gurnis, M., 2009. Emergence of a low-viscosity channel in subduction zones through the coupling of mantle flow and thermodynamics. Earth and Planetary Science Letters 278, 243–256.
Herrstrom, E.A., Reagan, M.K., Morris, J.D., 1995. Variations in lava composition associated with flow of asthenosphere beneath southern Central America. Geology 23 (7), 617–620.
Hirth, G., Kohlstedt, D.L., 1996. Water in the oceanic upper mantle; implications for rheology, melt extraction, and the evolution of the lithosphere. Earth and Planetary Science Letters 144 (1–2), 93–108.
Hochstaedter, A.G., Gill, J.B., Taylor, B., Ishizuka, O., Yuasa, M., Monta, S., 2000. Across-arc geochemical trends in the Izu Bonin arc: constraints on source composition and mantle melting. Journal of Geophysical Research 105, 495–512.
Hochstaedter, A., Gill, J.B., Peters, R., Broughton, P., Holden, P., 2001. Across-arc geochemical trends in the Izu–Bonin arc: contributions from the subducting slab. Geochemistry, Geophysics, Geosystems 2 2000GC000105.
Hofmann, A.W., 1988. Chemical differentiation of the Earth: the relationship between mantle, continental crust, and oceanic crust. Earth and Planetary Science Letters 90, 297–314.
Ishikawa, T., Tera, F., 1999. Two isotopically distinct fluids fluid components involved in the Mariana Arc; evidence from Nb/B ratios and B, Sr, Nd, and Pb isotope systematics. Geology 27, 83–86.
Iwamori, H., 1998. Transportation of H_2O and melting in subduction zones. Earth and Planetary Science Letters 160, 65–80.
Iwamori, I., 2007. Transportation of H2O beneath the Japan acs and its implications for global water circulation. Chemical Geology 239, 182–198.
Kelemen, P.B., Hirth, G., Shimizu, N., Spiegelman, M., Dick, H.J.B., 1997. A review of melt migration processes in the adiabatically upwelling mantle beneath oceanic spreading ridges. Philosophical Transactions of the Royal Society of London. A 355 (1723), 283–318.
Kelemen, P.B., Rilling, J.L., Parmentier, E.M., Mehl, L., Hacker, B.R., 2003. Thermal structure due to solid-state flow in the mantle wedge. Geophysical Monograph 138, 293–311.
Kelley, K.A., Plank, T., Grove, T.L., Stolper, E.M., Newman, S., Hauri, E., 2006. Mantle melting as a function of water content beneath back-arc basins. Journal of Geophysical Research 111 (B9), B09301.
Keppler, H., 1996. Constraints from partitioning experiments on the composition of subduction-zone fluids. Nature 380, 237–240.
Langmuir, C.H., Bezos, A., Escrig, S., Parman, S.W., 2006. Chemical systematics and hydrous melting of the mantle in back-arc basins. Geophysical Monograph 166, 87–146.
Leeman, W.P., Carr, M.J., Morris, J.D., 1994. Boron geochemistry of the Central American volcanic arc: constraints on the genesis of subduction-related magmas. Geochimica et Cosmochimica Acta 58, 149–168.
Magaritz, M., Taylor, H.P., 1974. Oxygen and hydrogen isotope studies of serpentinization in Troodos Ophiolite complex, Cyprus. Earth and Planetary Science Letters 23, 8–14.
McCulloch, M.T., Gamble, A.J., 1991. Geochemical and geodynamical constraints on subduction zone magmatism. Earth and Planetary Science Letters 102, 358–374.
Mysen, B.O., Boettcher, A.L., 1975. Melting of a hydrous mantle; II. Geochemistry of crystals and liquids formed by anatexis of mantle peridotite at high pressures and high temperatures as a function of controlled activities of water, hydrogen, and carbon dioxide. Journal of Petrology 16, 549–593.
Nakajima, J., Takei, Y., Hasegawa, A., 2005. Quantitative analysis of the inclined low-velocity zone in the mantle wedge of northeastern Japan: a systematic change of melt-filled pore shapes with depth and its implications for melt migration. Earth and Planetary Science Letters 234, 59–70.
Patino, L.C., Carr, M.J., Feigenson, M.D., 2000. Local and regional variations in Central American arc lavas controlled by variations in subducted sediment input. Contributions to Mineralogy and Petrology 138, 265–283.
Peacock, S.M., 1990. Fluid processes in subduction zones. Science 248, 329–337.
Peacock, S.M., van Keken, P.E., Holloway, S.D., Hacker, B.R., Abers, G.A., Ferguson, R.L., 2005. Thermal structure of the Costa Rica–Nicaragua subduction zone. Physics of the Earth and Planetary Interiors 149 (1–2), 187–200.
Pearce, J.A., Stern, R.J., Bloomer, S.H., Fryer, P., 2005. Geochemical mapping of the Mariana arc-basin system: implications for the nature and distribution of subduction components. Geochemistry, Geophysics, Geosystems 6 (7). doi:10.1029/2004GC000895.
Plank, T., Kelley, K., 2001. Contrasting sediment input and output at the Izu and Mariana subduction factories. EOS, Transactions, American Geophysical Union 82 (47), 1155.
Plank, T., Langmuir, C.H., 1988. An evaluation of the global variations in the major element chemistry of arc basalts. Earth and Planetary Science Letters 90 (4), 349–370.
Plank, T., Langmuir, C.H., 1993. Tracing trace elements from sediment input to volcanic output at subduction zones. Nature 362, 739–743.
Ranero, C.R., Phipps-Morgan, J., McIntosh, K., Reichert, C., 2003. Bending-related faulting and mantle serpentinization at the Middle America trench. Nature 425, 367–373.
Rüpke, L.H., Phipps-Morgan, J., Hort, M., Connolly, J., 2002. Are regional variations in Central American arc lavas due to differing basaltic versus peridotitic slab sources of fluids? Geology 30 (11), 1035–1038.
Rüpke, L.H., Phipps-Morgan, J., Hort, M., Connolly, J., 2004. Serpentine and the subduction water cycle. Earth and Planetary Science Letters 223, 17–34.
Ryan, J.G., Morris, J.D., Tera, F., Leeman, W.P., Tsvetkov, A., 1995. Cross-arc geochemical variations in the Kurile Arc as a function of slab depth. Science 270, 625–627.
Scambelluri, M., Rampone, E., Piccardo, G.B., 2001. Fluid and element cycling in subducted serpentinite: a trace-element study of the Erro-Tobbio high-pressure ultramafites (Western Alps, NW Italy). Journal of Petrology 42 (1), 55–67.
Schmidt, M.W., Poli, S., 1998. Experimentally based water budgets for dehydrating slabs and consequences for arc magma generation. Earth and Planetary Science Letters 163, 361–379.
Smith, P.M., Asimow, P.D., 2005. Adiabat_1ph: a new public front-end to the MELTS, pMELTS, and pHMELTS models. Geochemistry, Geophysics, Geosystems 6 (2), Q02004. doi:10.1029/2004GC000816.
Smith, P.M., Baker, L.J., Asimow, P.D., Gurnis, M., 2007. Coupled petrological and geodynamic models of mantle flow in subduction zones; the importance of chlorite in the emergence of a low-viscosity channel. Eos Transactions AGU 88 (52) Fall Meet. Suppl., Abstract V43D-1637.
Spiegelman, M., McKenzie, D., 1987. Simple 2-D models for melt extraction at mid-ocean ridges and island arcs. Earth and Planetary Science Letters 83, 137–152.
Staudigel, H., Davies, G.R., Hart, S.R., Marchant, K.M., Smith, B.M., 1995. Large-scale isotopic Sr, Nd and O isotopic anatomy of altered oceanic crust-DSDP/ODP sites 417/418. Earth and Planetary Science Letters 130, 169–185.
Stern, R.J., Fouch, M.J., Klemperer, S.L., 2003. In: Eiler, J. (Ed.), An Overview of the Izu–Bonin Mariana Subduction Factory: Geophysical Monograph, vol. 138, pp. 175–222.
Stern, R.J., Kohut, E.J., Bloomer, S.H., Leybourne, M., Fouch, M., Vervoot, J., 2006. Subduction factory processes beneath the Guguan cross-chain, Mariana Arc: no role for sediments, are serpentinites important? Contributions to Mineralogy and Petrology 151 (2), 202–221. doi:10.1007/s00410-005-0055-2.
Stolper, E.M., Newman, S., 1994. The role of water in the petrogenesis of Mariana Trough magmas. Earth and Planetary Science Letters 121, 293–325.
Straub, S.M., 2003. The evolution of the Izu Bonin–Mariana volcanic arcs (NW Pacific) in terms of major element chemistry. Geochemistry, Geophysics, Geosystems 4 (2), 1018. doi:10.1029/2002GC000357.
Taylor, B., 1992. Rifting and the volcanic–tectonic evolution of the Izu Bonin Mariana Arc. Proceedings of the Ocean Drilling Program. Scientific Results 126, 627–651.
Taylor, B., Martinez, F., 2003. Back-arc basin basalt systematics. Earth and Planetary Science Letters 210, 481–497.
Tenthorey, E., Hermann, J., 2004. Composition of fluids during serpentinite breakdown in subduction zones: evidence for limited boron mobility. Geology 32 (10), 865–868. doi:10.1130/G20610.
Ulmer, P., Trommsdorf, V., 1995. Serpentine stability to mantle depths and subduction-related magmatism. Science 268, 858–861.
Woodhead, J.D., Eggins, S.M., Gamble, J., 1993. High field strength and transition element systematics in island arc and back-arc basin basalts: evidence for multi-phase melt extraction and depleted mantle wedge. Earth and Planetary Science Letters 114, 491–504.
Woodhead, J.D., Hergt, J.M., Davidson, J.P., Eggins, S.M., 2001. Hafnium isotope evidence for 'conservative' element mobility during subduction zone processes. Earth and Planetary Science Letters 192, 331–346.
Workman, R.K., Hart, S.R., 2005. Major and trace element composition of the depleted MORB mantle (DMM). Earth and Planetary Science Letters 231 (1–2), 53–72 http://dx.doi.org/10.1016/j.epsl.2004.12.005.
Xu, Y., Wise, S.W., 1992. Middle Eocene to Miocene calcareous nanofossils of Leg 125 from the western Pacific Ocean. Proceedings of the Ocean Drilling Program. Scientific Results 125, 43–70.
Zhao, D.P., 2001. Seismological structure of subduction zones and its implications for arc magmatism and dynamics. Physics of the Earth and Planetary Interiors 127, 197–214.